NANO LETTERS

Letter

pubs.acs.org/NanoLett

Brightening of the Lowest Exciton in Carbon Nanotubes via Chemical Functionalization

Svetlana Kilina,[‡] Jessica Ramirez,[†] and Sergei Tretiak*[,§]

[†]Quantum Theory Project, University of Florida, Gainesville, Florida 32611, United States

[‡]Department of Chemistry and Biochemistry, North Dakota State University, Fargo, North Dakota 58108, United States

[§]Theoretical Division, Center for Nonlinear Studies (CNLS) and Center for Integrated Nanotechnologies (CINT), Los Alamos National Laboratory, Los Alamos, New Mexico 87545, United States

Supporting Information

ABSTRACT: Using time-dependent density functional theory, we found that chemical functionalization at low concentrations of single-walled carbon nanotubes (SWNTs) locally alters the π-conjugated network of the nanotube surface and leads to a spatial confinement of the electronically excited wave functions. Depending on the adsorbant positions, the chemisorption significantly modifies the optical selection rules. Our modeling suggests that photoluminescent efficiency of semiconducting SWNT materials can be controlled by selective chemical functionalization.

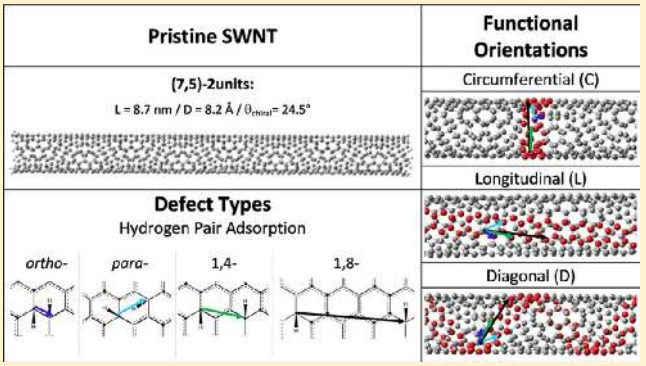

KEYWORDS: *Single-walled carbon nanotubes (SWNTs), time-dependent density functional theory (TDDFT), photoluminescent (PL), exciton, chemisorption*

A variety of low-dimensional materials are highly photoluminescent (PL). For example, conjugated polymers,[1] semiconductor nanowires, and quantum dots[2] may exhibit near-unity (~100%) quantum yield (QY). In this respect, semiconducting single-wall carbon nanotubes (SWNTs) are drastically different initially showing only 10^{-3}–10^{-4} PL efficiency.[3] Such low luminescence of macroscopic SWNT samples is attributed to the presence of tube bundles, metallic tubes, and tubes with multiple defects, which quench emission.[4,5] However, even the high quality SWNT ensembles[6,7] and individual SWNTs still have overall low PL efficiency: a few percent or less in water[5,8,9] and up to 20% in organic solvents.[10] Low PL efficiency of semiconducting SWNTs is attributed to the intrinsic low-lying optically forbidden ("dark") states[11−15] and fast exciton mobility to the quenching sites.[16,17] The lower-energy optical excitations in SWNTs have been ascertained as originating from four exciton subbands[18] with three dark excitons residing below the first optically allowed bright E_{11} excitons.[11,12,19,20] The existence of the lowest-energy dark excitons has been explicitly verified via time-resolved spectroscopy,[21] two photon spectroscopy,[22] and PL spectroscopy in the presence of high magnetic fields altering the optical selection rules.[23−25] The excitonic structure and dynamics in SWNTs, however, is even more complicated by the presence of triplet excitons[14,26] and dark or semibright (weakly optically allowed) cross-polarized E_{12} excitonic bands in between the bright E_{11} and E_{22} transitions.[27−29]

Despite excitonic state complexity and low PL efficiency, optical properties of semiconducting SWNTs have multiple advantages over other nanomaterials. For example, SWNTs exhibit size-tunable, stable, and nonblinking (at room temperature) fluorescence at near-infrared (NIR) wavelength[30] and narrow homogeneous line width.[31] Such robust photophysical features are important for a number of fluorescent-based applications, including bioimaging[32,33] and biosensing.[34] The unique ability of a SWNT to emit a single photon at low temperatures with NIR wavelength is promising for applications in quantum cryptography[35] and optoelectronics.[36] Hence overcoming intrinsic limitations and making highly luminescent SWNTs materials will immediately allow for many new applications and emerging technologies.

Chemical functionalization of the nanotube surface offers an attractive route to change the selection rules governing the optical activity in SWNTs. For example, recent experiments on individual SWNTs in water have revealed significant increase in PL efficiency upon addition of reducing agents, such as dithiothreitol and others.[37] Low-energy satellite PL peaks with energies and PL efficiency dependent on the nanotube surroundings have been found in SWNTs ensembles and individual samples.[21,38,39] Other experimental studies have

Received: January 13, 2012
Revised: March 9, 2012
Published: April 11, 2012

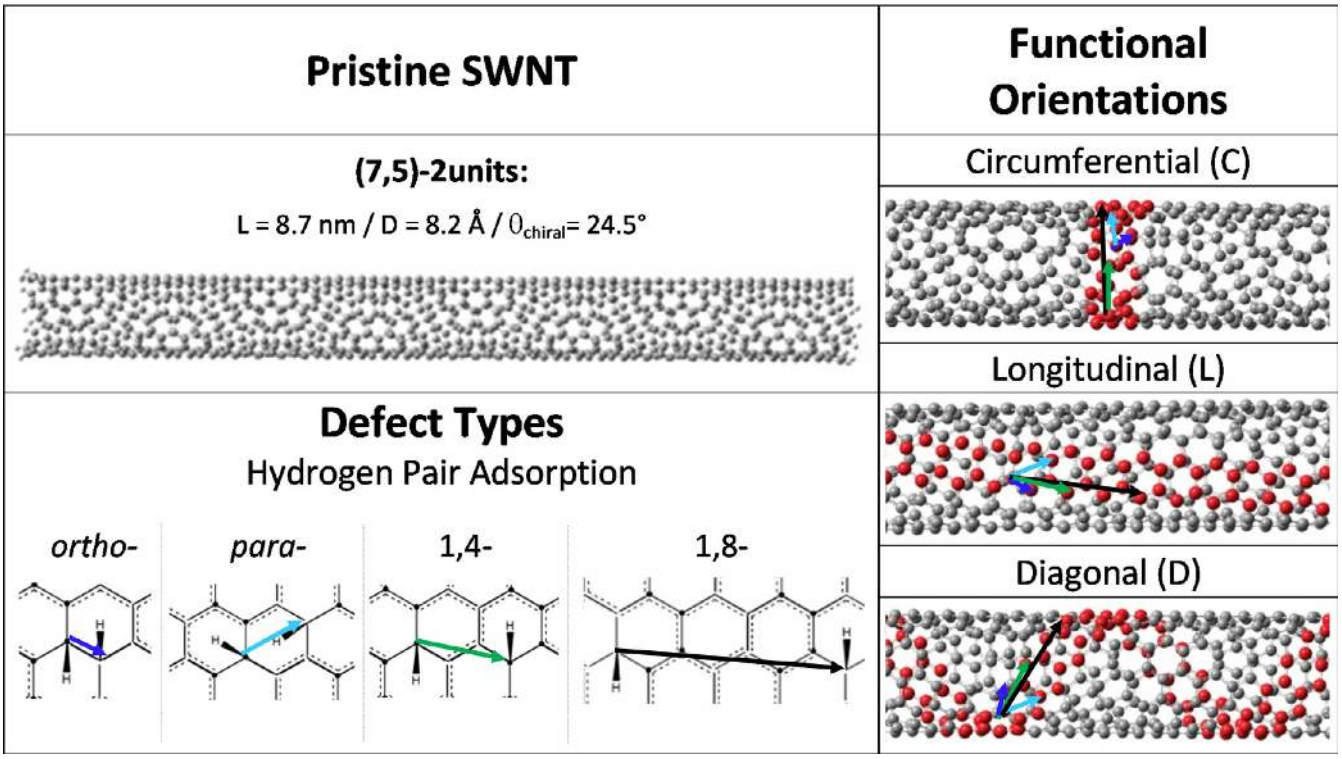

Figure 1. The upper left panel shows the geometry and structural parameters of the pristine (7,5) two-unit SWNT. The lower left panel illustrates the types of hydrogen defects studied. The *ortho-* and *para-* defects originate from two atomic hydrogens attached to a single carbon ring on the nanotube surface, while 1,4- and 1,8- defects are associated with hydrogens bonded to different carbon rings. Possible orientations of these defects with respect to the nanotube axis are shown in the right panels: circumferential (C), perpendicular to the *z*-axis; longitudinal (L), nearly parallel to the *z*-axis; and diagonal (D), following a chiral angle. The diagonal direction illustrates the chirality θ_{chiral} of the tube (7,5), and the coiling angle of the red line D corresponds to the θ_{chiral} = 24.5 degrees, if measured with respect to the tube edge, or 65.5 degrees if measured relative to the tube axis. Only two hydrogens are adsorbed along each direction resulting in 0.2% adsorbate concentrations in SWNT. The positions of the hydrogens are marked by an arrow of a color corresponding to *ortho-* (blue), *para-* (cyan), 1,4- (green), and 1,8- (black) defects.

reported the appearance of low-energy satellite PL peaks in samples exposed to intense pulsed-laser irradiation, which creates local defects within the nanotube structure.[40,41] Analogous to the effect of the strong pulsed-laser beam, the adsorption of atomic gold[40] and hydrogen[42] onto a SWNT surface has been observed to cause the rising intensity of satellite peaks at the lower-energy end of the PL spectra. Red-shifted satellite peaks have been also observed in PL spectra of covalently oxygen-doped nanotubes prepared by exposure to ozone and then light.[43] Such brightening of satellite PL peaks has been associated with distortions of nanotube structures due to local chemical defects that induce mixing between bright and dark excitons.[40,43] In contrast, a significant reduction in the PL efficiency has been found for protonated SWNTs[44] and SWNT dispersions exposed to acidic environments.[45,46] The PL quenching of functionalized tubes has been explained by the presence of hole trap states originated from chemical defects.[37] Alternative hypotheses have suggested involvement of triplet states that provide bright red-shifted satellite peaks in emission.[40−42] Thus, the mechanisms that enable optically forbidden transitions and the interplay between bright and dark excitons in SWNTs upon chemical fictionalization remain to be clarified.

In this Letter we theoretically address the question of whether a local chemical defect on the nanotube surface due to atomic hydrogen adsorption can brighten the lowest excitonic state and, thus, enhance the PL efficiency in SWNTs. Time dependent density functional theory (TDDFT) modeling allows us to analyze how such functionalization impacts optical transitions and excitonic wave functions of bright/dark states in comparison to the pristine tube electronic structure. Our results suggest that low concentrations of hydrogen atoms adsorbed to the nanotube sidewalls can significantly perturb the π-conjugated electronic system, resulting in a spatially confined excited state wave function in the near-vicinity of the dopant atom sites. Consequently, the chemisorption modifies optical selection rules, frequently resulting in brightening and energy red-shifts of the lowest excited state, compared to the first excitonic subband of the pure SWNTs. The magnitude of this effect is strongly dependent on the orientation, concentration, and charge state of the added functional groups. The tube chirality is shown to have a lesser influence on the observed trends.

We focus on four narrow diameter (<1 nm) semiconducting SWNTs with chirality indices (6,2), (6,5), (7,5) and (7,6), which are frequently used in experimental measurements. Here we analyze in detail results for the (7,5) series. Very similar trends are observed for the other three species. Computational data for the latter are presented in the Supporting Information (Figure S1) and are summarized in Figure 4. Nanotube structures of about 10 nm in length were constructed using integer values of unit cells to preserve the natural tube symmetry. Dangling bonds at the truncated tube-ends were passivated with hydrogen atoms, as detailed elsewhere,[47] to avoid spurious end-effects and introduction of edge states into the band gap of nanotubes. Such a "molecular-type" approach,

dx.doi.org/10.1021/nl300165w | *Nano Lett.* 2012, 12, 2306−2312

which assumes analysis of finite-size nanotubes with length larger than the exciton size (the characteristic distance between photoexcited electron and hole being ~2−3 nm), was previously successful in studies of pristine nanotubes.[14,15,28,47,48] In our case, the SWNTs are at least 3 times larger than the exciton size, which allows our computational results to be free of confinement effects and to reproduce trends in the infinite-length tubes.[14,15,28,47,48] For example, calculated oscillator strengths of delocalized excited states in the pristine tube is proportional to the length of the tube segment.

To introduce a chemical defect, two hydrogen atoms were bound to the surface approximately in the middle of the tube, resulting in 0.2% adsorbate concentrations (two hydrogens per 1000 carbons of nanotube) corresponding to low densities of adsorbates used in experiments.[40,43] Hydrogens have been attached to carbons over one, three, and seven C−C bonds to maintain aromaticity (see Figure 1). In all cases, adsorbants locally perturb π-conjugation by introducing partial sp^3 bonding character for the respective carbons bound to H atoms.[49] The *ortho-* and *para-* defects constrain the bonding sites to lie within a single benzene ring along the SWNT sidewall, whereas the 1,4- and 1,8- defects allow for bonding separated by multiple rings. In addition, we have considered several possible orientational alignments for the added hydrogen atoms, with respect to the nanotube chiral vector, as illustrated in Figure 1. Even though we use a very simple adsorbant, similar modifications to the π-electron conjugation network are expected upon covalent bonding of other chemical agents to the SWNT sidewalls.[49]

All geometries (pristine tubes and tubes with adsorbed hydrogens) were optimized using the semiempirical AM1[50] Hamiltonian, as implemented within the Gaussian 09 package.[51] The AM1 geometries were further compared against those obtained at the PM6[52] level of theory, demonstrating an excellent agreement for bond lengths between both methods. In all electronic structure calculations, we have preserved neutral charge and singlet multiplicity of molecular systems. Subsequent excited-state calculations were carried out using the TDDFT approach. It was shown before that hybrid functionals (including a fraction of orbital exchange into kernel) allow for the accurate description of bound excitonic states in conjugated organic materials[53] and, in particular, carbon nanotubes.[14,15] Therefore, we have used the B3LYP model[54] for the majority of our calculations. To check that artificial charge-transfer states are not present in the B3LYP results, especially in the case of covalently functionalized nanotubes, excited states were also calculated using the long-range corrected CAM-B3LYP[55] functional. Overall, both approaches provide similar results barring consistent blue-shifts in spectra obtained with CAM-B3LYP approach (see Figure S2 in the Supporting Information). The minimal STO-3G basis set was utilized in all TDDFT calculations. The 25 lowest singlet excited-state transition energies and their respective oscillator strengths were obtained for each molecular system in the output of a TDDFT calculation. The calculated oscillator strengths and transition energies were used to simulate the absorption spectra and the radiative lifetime in SWNTs (eq 1 in the Supporting Information). The absorption spectra were obtained using Gaussian line shape with an empirical line-broadening parameter of 0.01 eV to mimic various broadening effects occurring under experimental conditions. Finally, the spatial extents of excited state wave functions have been analyzed using natural transition orbitals (NTOs)[56] and two-dimensional plots of transition density matrices, representing the electronic transition between the ground state and electronically excited states.[14,15]

Figure 2a shows calculated absorption spectra for the five (7,5) SWNT species, namely the pristine tube and tubes with

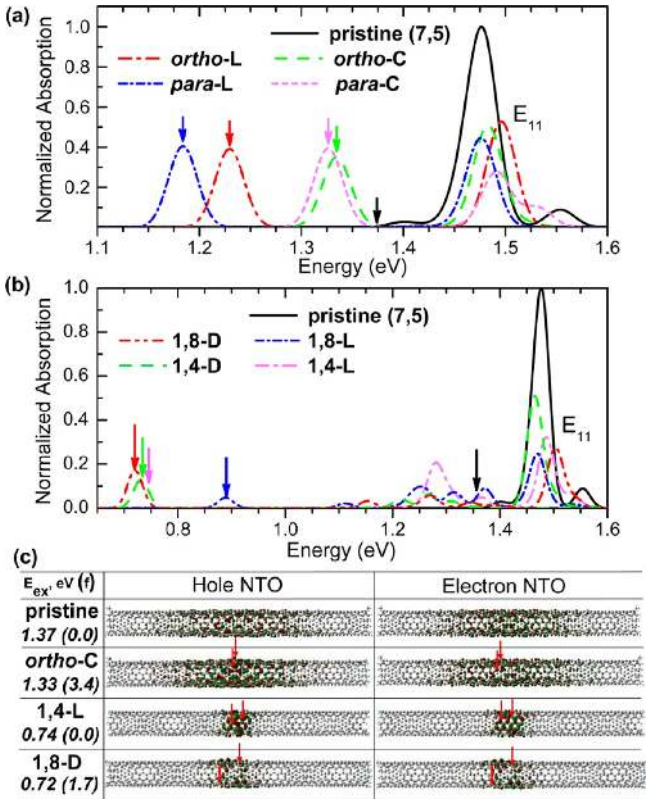

Figure 2. Comparison of calculated optical properties of hydrogenated and pristine (7,5) SWNT systems. (a) Absorption spectra with the *ortho-* and *para-* positions of hydrogen pair placed at circumferential (C) and longitudinal (L) orientations; (b) Absorption spectra with the 1,4- and 1,8- positions of hydrogen pair placed at diagonal (D) and longitudinal (L) orientations. Energy corresponding to the first excitation of each system is indicated by a vertical arrow. (c) Representative electron and hole NTOs corresponding to the lowest excited state of pristine and hydrogenated (7,5) SWNT systems. To the left of each NTO pair, the corresponding transition energy (eV) and oscillator strength (in parentheses) are given. The red arrows mark the position of adsorbed hydrogens.

two hydrogens adsorbed at *ortho-* and *para-* positions following circumferential and longitudinal orientations with respect to the tube axis (see Figure 1). The pristine nanotube has a single strong E_{11} absorption peak at ~1.47 eV. The lowest state (dark exciton) shown by an arrow in Figure 2 has negligible oscillator strength in agrement with previous theoretical studies.[11−15] In all hydrogenated species, the E_{11} exciton energy changes insignificantly upon functionalization, most commonly seen as a slight blue-shift of the E_{11} peak compared to the pristine tube. However, its intensity is dramatically reduced compared to that in pristine tube. Simultaneously, an intense red-shifted peak associated with the lowest excited state in SWNT appears in the spectra of tubes hydrogenated at *ortho-* and *para-* positions having roughly the same oscillator strength as the E_{11} peak. Integration of the oscillator strength over the energy range of 0.6−1.6 eV for the pristine and functionalized (7,5) SWNTs

dx.doi.org/10.1021/nl300165w | Nano Lett. 2012, 12, 2306−2312

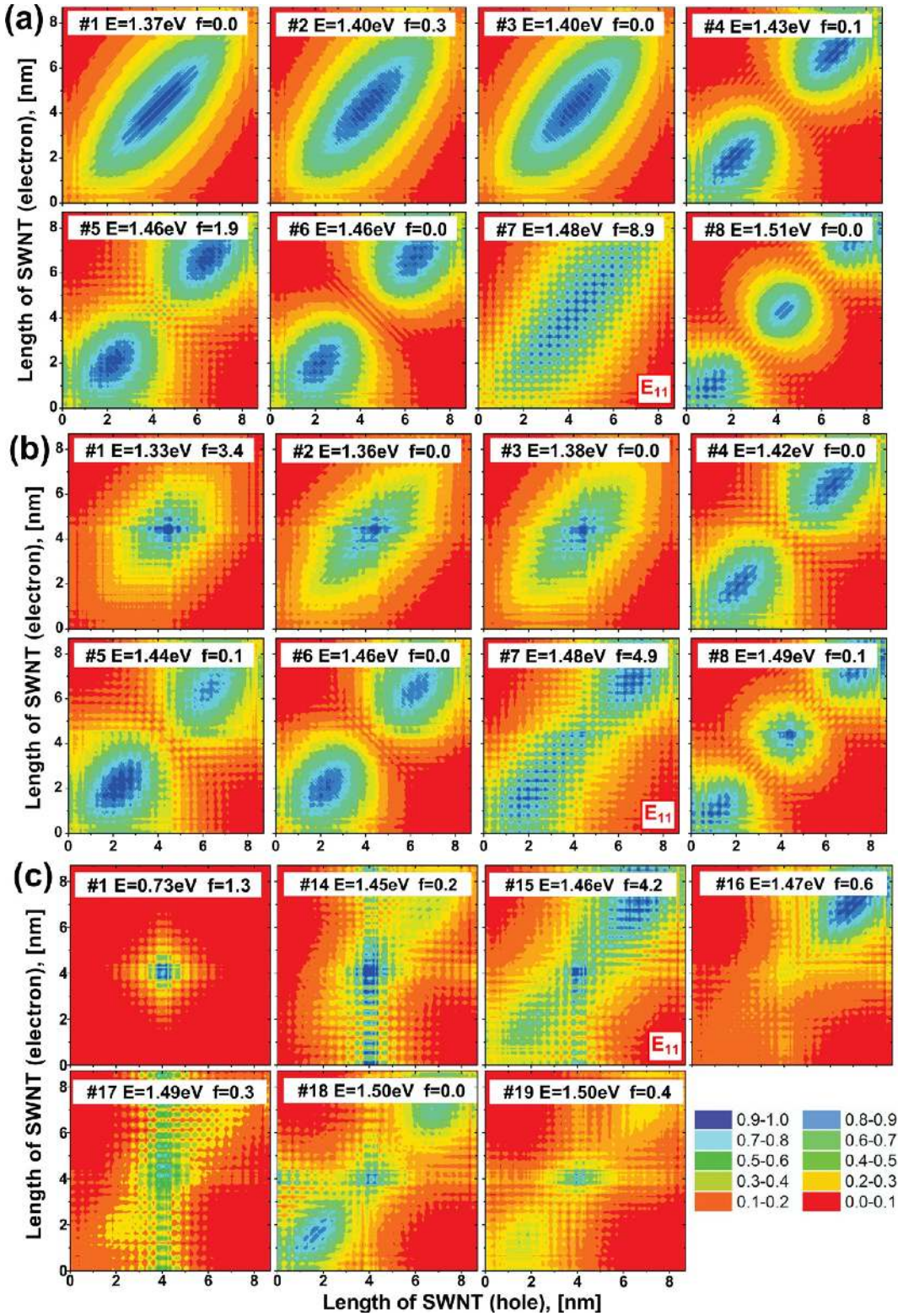

Figure 3. Contour two-dimensional plots of transition density matrices corresponding to optically relevant excited states are shown for (a) pristine, (b) *ortho*-C adsorbate position, and (c) 1,4-D adsorbate position in (7,5) SWNT systems. The location of defects corresponds to the point on the diagonal at about 4−5 nm along the *X*- and *Y*-axes (middle of the nanotube). Each plot depicts probabilities of an electron moving from one molecular position (*X*-axis) to another (*Y*-axis) upon electronic excitation. The color code is shown in the bottom right panel. Each panel also gives a state number, its transition energy (eV), and strength, *f*. For the case depicted in c, states 2−13 (not shown) correspond to either localized transitions or excitations with strong change transfer character.

results in a constant value independent of the introduced defects. This indicated the redistribution of the oscillator strength between the E_{11} excitonic band and defect-associated states. Thus, as follows from Figure 2a, significant brightening of the lowest exciton and the concurrent lowering of the oscillator strength of the bright E_{11} state occurs for the tubes

dx.doi.org/10.1021/nl300165w | *Nano Lett.* 2012, 12, 2306−2312

with hydrogens adsorbed on the same carbon ring. These results suggest that observed excitonic brightening should be noticeable in experiments as an additional red-shifted emissive peak. We note that the computed gap between the E_{11} peak and the lowest excited state brightened upon hydrogen adsorption on *para-* and *ortho-* positions varies significantly for all molecular systems considered (see Figure 2a). These calculated splittings (~70−320 meV) are comparable with splittings between the main E_{11} and satellite peaks experimentally measured in samples exposed to intense pulsed-laser irradiation[40,41] (~106−220 meV) and in oxygen-doped SWNTs[43] (~106−220 meV). A smaller energy difference (~40−80 meV) has been observed for the larger diameter (≥1 nm) SWNTs under atomic hydrogen exposure.[42] These experiments also show that such splittings increase with a decrease of the tube diameter and depend on the tube chirality.

Figure 2b shows calculated absorption spectra for the five (7,5) SWNT species, namely, the pristine tube and tubes with two hydrogens adsorbed on 1,4- and 1,8-sites following diagonal and longitudinal orientations with respect to the tube axis (see Figure 1). Similar to the previous case, we observe a significant reduction of the E_{11} absorption peak intensity in all hydrogeneted tubes compared to the pristine tube. However, the optical intensity is dispersed among multiple excited states. Consequently, the lowest exciton state gains small oscillator strength in all cases considered. Moreover, for these functionalizations, the splittings between the E_{11} peak and the lowest excited state appearing due to hydrogen adsorption is very large (about 0.6−0.7 eV). These computational results suggest weaker and significantly red-shifted PL, which may be further quenched due to environmental effects given the localized nature of the emitting state (see Figure 2c) and small transition energy.

To analyze the observed trends, we further examine the electron and hole NTOs[56] and transition density matrices showing spatial delocalization of the excitonic wave functions. Figure 2c displays representative NTOs for pristine and hydrogeneted tubes corresponding to the lowest excited state. As expected, both electron and hole orbitals in the pristine tube are delocalized across the entire system. Additionally, transition density matrices (Figure 3a) computed for several low-energy excited states demonstrate a characteristic standing wave structure of excitons, where the number of nodes in the charge density along the plot diagonal is related to the exciton momenta.[57] For the finite system considered here, the dispersion (dependence of the exciton energy on the k-vector) is not continuous: The bands consist of discrete excited states where every state can be associated with a specific momentum (k-vector) in the infinite tube length limit. Thus, four node-less states (1, 2, 3, and 7) correspond to the fundamental four excitonic bands of the first Van-Hove singularity, including three dark and one bright E_{11} states. Each of these excitons has its sub-band of states with higher momenta having one or more nodes in their transition densities (see detailed analysis elsewhere[14,15,21]).

Hydrogenation in the *ortho-* and *para-* positions leads to a slight localization of the NTOs to the vicinity of the chemisorbed hydrogens, as well as small increases in the electron and hole orbital density around the defect (Figure 2c and Figure S3 in the Supporting Information). Consequently, such functionalization results in the appearance of delocalized defect states, as supported by the transition density matrices of the low-energy excited states shown in Figure 3b. All excitons presented in the pristine tube (Figure 3a) are also recognizable in the tube with hydrogens adsorbed on a single ring (Figure 3b). The first three sub-bands have noticeable localization around the chemical defect in the center of a tube. Compared to the pristine tube, the structure of the bright E_{11} state (7) is markedly different: the transition density drops its amplitude near the chemical defect; thus, the lowest and E_{11} state wave functions become spatially separated. Consequently, the lowest state (dark in the pristine tube) shows a significant oscillator strength, while E_{11} exciton decreases optical intensity, compared to the pristine tube. To rationalize this effect, we invoke an analogy with excited states of a molecular dimer, where coupled chromophores (and their transition dipole moments) are parallel to each other (H-aggregate arrangement). In this case, the wave functions of the dimer excited states are superpositions of the monomer wave functions.[58,59] The lowest state is optically dark (antisymmetric combination), and the second state (symmetric combination) is bright by gaining the oscillator strength from both molecules. We can impose this simplistic model onto SWNTs where a degenerate two pairs of molecular orbitals appearing due to tube symmetry mix in pristine tubes leading to the lowest dark state (antisymmetric superposition) and the higher bright E_{11} state (symmetric superposition).[11] The splitting between dark and bright states reflects Coulombic coupling and electron correlation effects. The other two excitonic subbands formally correspond to the intermolecular charge transfer transitions. Chemical functionalization that alters excited state energies of one monomer may efficiently decouple states in the molecular dimer by breaking wave function superpositions so that the resulting excited states would be localized back on their parent molecules and both would be optically active. This is precisely what we observe in hydrogenated SWNTs (compare transition density plots for states 1 and 7 in Figure 3b).

In contrast to the above case, attachment of hydrogens to different carbon rings on the tube surface (1,4- and 1,8-defects) results in a significant red-shift of the lowest excitonic transition, the wave function of which becomes highly localized with an electron and a hole being "trapped" between the two bonding hydrogen atoms, as can be seen from NTOs (Figure 2c and Figure S3 in the Supporting Information) and transition densities (Figure 3c). Such strong spatial localization explains small oscillator strength of this transition, compared to the *ortho-* and *para-* cases, and even complete darkening of the lowest state depending on the defect orientation (circumferential, longitudinal, or diagonal). Consequently, this scenario can be interpreted from a traditional semiconductor physics viewpoint, where the defect states are localized and energetically located near the midgap of the material as was recently shown for SWNTs doped with $AuCl_3$.[17] Compared to the pristine tube, the structure of the other excitonic states is also significantly changed (Figure 3c). These differences in the exciton transition densities suggest that adsorbates on different carbon rings trap the excitation with new defect-localized low-energy states, which might be weakly optically allowed or completely dark depending on the defect orientation with respect to the tube axis (see spectra in Figure 2b).

Similar trends in modification of optical absorption and excitonic structure upon hydrogen adsorption have been observed for all four SWNTs we considered (see Figure S1 in the Supporting Information). Figure 4 summarizes our calculations in terms of the splittings between the lowest-energy and bright E_{11} states calculated for four types of the pristine and

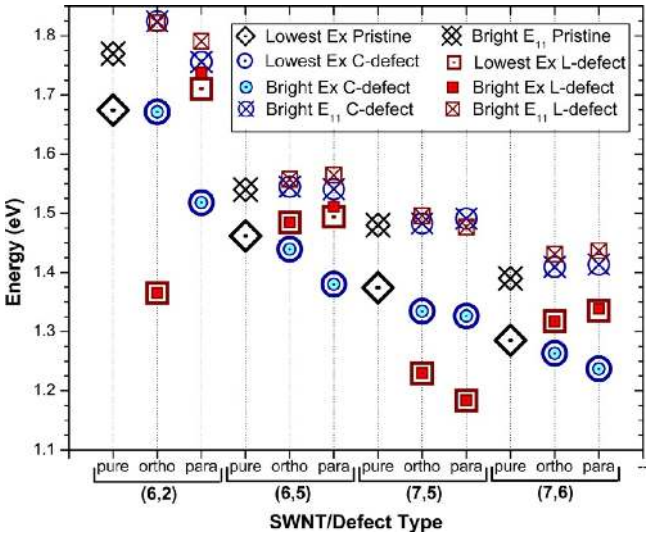

Figure 4. Positions of bright and dark excitons calculated for four nanotube chiralities are shown to facilitate a comparison of dark-bright energy splittings (in eV) across series. Three columns appear for each nanotube type (from left to right): the first column shows the dark (the lowest) and bright E_{11} excitons in pristine tubes; the second column shows the lowest-energy, first bright, and E_{11} excitons for the corresponding *ortho-* circumferentially (C) and longitudinally (L) functionalized systems; the third column shows the same data as the previous column, but for the *para-* type systems. When filled and empty circles or squares coincide, the lowest exciton is optically active. *Ortho-* defects always lead to the brightening of the lowest excitonic state in SWNTs.

hydrogenated tubes (only *ortho-* and *para-* positions for circumferential and longitudinal defect orientations are shown). In all cases, the bright E_{11} exciton is only slightly perturbed by functionalization, showing an insignificant blue shift relative to the E_{11} peak in the pristine SWNTs. Save for two exceptions (the *para*-longitudinal defects in the smallest (6,2) and (6,5) tubes), hydrogenation leads to a brightening of the lowest state of nantubes. According to eq 1 in the Supporting Information and the calculated oscillator strength and energy of the lowest optically allowed transition, we can estimate the radiative lifetime of the functionalized nanotube. For considered SWNTs, the radiative lifetime is about 7−15 ns depending on the tube chirality and the position of the chemical defect. These times are comparable to the typical radiative lifetime of highly luminescent organic conjugated molecules (10 ns). Overall, the magnitude of the red-shift and the oscillator strength of the lowest state, as compared to the primary bright E_{11} exciton, and consequently an appearance of a satellite red-shifted peak in PL are controlled by the type and orientation of the absorbed chemical defect, and, to a lesser degree, by tube chirality.

In summary, we have demonstrated that covalent functionalization of SWNTs introduces local sp^3 bond character along the otherwise conjugated sp^2 carbon network of the nanotube sidewall, resulting in a partial or complete localization of excitonic wave functions in the vicinity of the defect site. Chemical defects originating from hydrogen adsorption on a single carbon ring perturb the low-energy excitonic band, allowing the lowest-lying excited state to moderately red-shift (~70−200 meV) and to gain substantial oscillator strength, leading to an enhanced PL potential. Moreover, such low-lying semilocalized excited states will efficiently limit excitonic diffusion, potentially routing excitons to emission quenching sites,[16,17] by pinning excitons to the fluorescing defect sites, and, thus, further facilitating the PL efficiency. Such immobilization of the emitting species has been recently shown for trion PL in SWNTs.[60] The other functionalization patterns explored (1,4- and 1,8-cases) result in new highly localized states, which are only weakly optically allowed or completely optically forbidden depending on the defect orientation. Considered covalent functionalizations are already exploited in relevant to SWNTs materials. For example, the *ortho-* type is common for a variety of fullerenes such as PCBM, a derivative of the C_{60} buckyball often used in plastic solar cells. Thus, through development of synthetic techniques[49] precisely controlling binding and orientation of covalent functionalization on semiconducting SWNTs, adsorbates may be used to enhance the PL efficiency of these materials.

■ ASSOCIATED CONTENT

Supporting Information

Discussion on oscillator strength and radiative lifetime; absorption spectra of hydrogenated (6,2), (6,5), and (7,6) SWCNTs; comparison of absorption spectra of a hydrogenated (7,5) SWNT calculated by B3LYP and CAM-B3LYP functionals; representative electron and hole NTOs corre- sponding to the lowest excited state of pristine and hydrogenated (7,5) SWNT systems. This material is available free of charge via the Internet at http://pubs.acs.org.

■ AUTHOR INFORMATION

Corresponding Author

*E-mail: serg@lanl.gov.

Notes

The authors declare no competing financial interest.

■ ACKNOWLEDGMENTS

The authors thank Bruce Weisman, Juan Duque, and Steven Doorn for fruitful discussions. S.K. acknowledges financial support from NDSU Advance FORWARD program sponsored by NSF HRD-0811239 for the renovated Lab space and ND EPSCoR through NSF grant #EPS-0814442. S.T. and J. R. acknowledge support of the U.S. Department of Energy and Los Alamos National Laboratory (LANL) Directed Research and Development funds. We also acknowledge the support of the Center for Integrated Nanotechnology (CINT) and Center for Nonlinear Studies (CNLS) at LANL. LANL is operated by Los Alamos National Security, LLC, for the National Nuclear Security Administration of the U.S. Department of Energy under Contract DE-AC52-06NA25396.

■ REFERENCES

(1) Gunes, S.; Neugebauer, H.; Sariciftci, N. *Chem. Rev.* **2007**, *107*, 1324−1338.
(2) Nozik, A. J. *Annu. Rev. Phys. Chem.* **2001**, *52*, 193.
(3) O'Connell, M. J.; Bachilo, S. M.; Huffman, C. B.; Moore, V. C.; Strano, M. S.; Haroz, E. H.; Rialon, K. L.; Boul, P. J.; Noon, W. H.; Kittrell, C.; Ma, J. P.; Hauge, R. H.; Weisman, R. B.; Smalley, R. E. *Science* **2002**, *297*, 593.
(4) Bachilo, S. M.; Strano, M. S.; Kittrell, C.; Hauge, R. H.; Smalley, R. E.; Weisman, R. B. *Science* **2002**, *298*, 2361−2366.
(5) Jones, M.; Engtrakul, C.; Metzger, W. K.; Ellingson, R. J.; Nozik, A. J.; Heben, M. J.; SRumbles, G. *Phys. Rev. B* **2005**, *71*, 115426−1−9.
(6) Tsyboulski, D. A.; Rocha, J. D. R.; Bachilo, S. M.; Cognet, L.; Weisman, R. B. *Nano Lett.* **2007**, *7*, 3080−3085.

(7) Fantini, C.; Cassimiro, J.; Peressinotto, V.; Plentz, F.; Filho, A. S.; Furtado, C.; Santos, A. *Chem. Phys. Lett.* **2009**, *473*, 96−101.
(8) Crochet, J.; Clemens, M.; Hertel, T. *J. Am. Chem. Soc.* **2007**, *129*, 8058−8059.
(9) Carlson, L. J.; Maccagnano, S. E.; Zheng, M.; Silcox, J.; Krauss, T. D. *Nano Lett.* **2007**, *7*, 3698−3703.
(10) Ju, S. Y.; Kopcha, W. P.; Papadimitrakopoulos, F. *Science* **2009**, *323*, 1319−1323.
(11) Zhao, H. B.; Mazumdar, S. *Phys. Rev. Lett.* **2004**, *93*, 157402.
(12) Perebeinos, V.; Tersoff, J.; Avouris, P. *Nano Lett.* **2005**, *5*, 2495.
(13) Spataru, C. D.; Ismail-Beigi, S.; Benedict, L. X.; Louie, S. G. *Phys. Rev. Lett.* **2005**, *95*, 247402.
(14) Tretiak, S. *Nano Lett.* **2007**, *7*, 2201−2206.
(15) Kilina, S.; Badaeva, E.; Piryatinski, A.; Tretiak, S. *Phys. Chem. Chem. Phys.* **2009**, *11*, 4113−4123.
(16) Harrah, D. M.; Swan, A. K. *ACS Nano* **2011**, *5*, 647−655.
(17) Crochet, J. J.; Duque, J. G.; Werner, J. H.; Doorn, S. K. *Nat. Nanotechnol.* **2012**, *7*, 126−132.
(18) Ando, T. *J. Phys. Soc. Jpn.* **1997**, *66*, 1066.
(19) Wang, F.; Dukovic, G.; Brus, L. E.; Heinz, T. F. *Science* **2005**, *308*, 838−841.
(20) Maultzsch, J.; Pomraenke, R.; Reich, S.; Chang, E.; Prezzi, D.; Ruini, A.; Molinari, E.; Strano, M. S.; Thomsen, C.; Lienau, C. *Phys. Rev. B* **2005**, *72*, 241402.
(21) Scholes, G. D.; Tretiak, S.; McDonald, T. J.; Metzger, W. K.; Engtrakul, C.; Rumbles, G.; Heben, M. J. *J. Phys. Chem. C* **2007**, *111*, 11139−11149.
(22) Wang, F.; Dukovic, G.; Brus, L. E.; Heinz, T. F. *Phys. Rev. Lett.* **2004**, *92*, 177401.
(23) Zaric, S.; Ostojic, G. N.; Kono, J.; Portugall, O.; Frings, P. H.; Rikken, G. L. J. A.; Furis, M.; Crooker, S. A.; Wei, X.; Moore, V. C.; Hauge, R. H.; Smalley, R. E. *Phys. Rev. Lett.* **2006**, *96*, 016406.
(24) Shaver, J.; Kono, J.; Portugall, O.; Krstić; Rikken, G. L. J. A.; Miyauchi, Y.; Maruyama, S.; Perebeinos, V. *Nano Lett.* **2007**, *7*, 1851−1855.
(25) Srivastava, A.; Htoon, H.; Klimov, V. I.; Kono, J. *Phys. Rev. Lett.* **2008**, *108*, 087402.
(26) Mohite, A. D.; Santos, T. S.; Moodera, J. S.; Alphenaar, B. W. *Nat. Nanotechnol.* **2009**, *4* (7), 425−429.
(27) Luo, Z. T.; Papadimitrakopoulos, F.; Doorn, S. K. *Phys. Rev. B* **2007**, *75*, 205438.
(28) Kilina, S.; Tretiak, S.; Doorn, S. K.; Luo, Z.; Papadimitrakopoulos, F.; Piryatinski, A.; Saxena, A.; Bishop, A. R. *Proc. Natl. Acad. Sci. U.S.A.* **2008**, *105*, 6797−6802.
(29) Miyauchi, Y.; Ajiki, H.; Maruyama, S. *Phys. Rev. B* **2010**, *81*, 121415−1−4.
(30) Hartschuh, A.; Pedrosa, H. N.; Novotny, L.; Krauss, T. D. *Science* **2003**, *301*, 1354−1356.
(31) Htoon, H.; O'Connell, M. J.; Cox, P. J.; Doorn, S. K.; Klimov, V. I. *Phys. Rev. Lett.* **2004**, *93*, 027401.
(32) Heller, D. A.; Baik, S.; Eurell, T. E.; Strano, M. S. *Adv. Mater.* **2005**, *17*, 2793−2799.
(33) Leeuw, T. K.; Reith, R. M.; Simonette, R. A.; Harden, M. E.; Cherukuri, P.; Tsyboulski, D. A.; Beckingham, K. M.; Weisman, R. B. *Nano Lett.* **2007**, *7*, 2650−2654.
(34) Zhang, J.; Boghossian, A. A.; Barone, P. W.; Rwei, A.; Kim, J.; Lin, D.; Heller, D. A.; Hilmer, A. J.; Nair, N.; Reuel, N. F.; Strano, M. S. *J. Am. Chem. Soc.* **2011**, *133*, 567−581.
(35) Högele, A.; Galland, C.; Winger, M.; Imamoğlu, A. *Phys. Rev. Lett.* **2008**, *100*, 217401−1−4.
(36) Avouris, P.; Chen, Z. H.; Perebeinos, V. *Nat. Nanotechnol.* **2007**, *2*, 605.
(37) Lee, A. J.; Wang, X.; Carlson, L. J.; Smyder, J. A.; Loesch, B.; Tu, X.; Zheng, M.; Krauss, T. D. *Nano Lett.* **2011**, *11*, 1636−1640.
(38) Kiowski, O.; Arnold, K.; Lebedkin, S.; Hennrich, F.; Kappes, M. M. *Phys. Rev. Lett.* **2007**, *99*, 237402−1−4.
(39) Lebedkin, S.; Hennrich, F.; Kiowski, O.; Kappes, M. M. *Phys. Rev. B* **2008**, *77*, 165429−1−8.
(40) Harutyunyan, H.; Gokus, T.; Green, A. A.; Hersam, M. C.; Allegrini, M.; Hartschuh, A. *Nano Lett.* **2009**, *9*, 2010−2014.
(41) Matsunaga, R.; Matsuda, K.; Kanemitsu, Y. *Phys. Rev. B* **2010**, *81*, 033401.
(42) Nagatsu, K.; Chiashi, S.; Konabe, S.; Homma, Y. *Phys. Rev. Lett.* **2010**, *105*, 157403.
(43) Ghosh, S.; Bachilo, S. M.; Simonette, R. A.; Beckingham, K. M.; Weisman, R. B. *Science* **2010**, *330*, 1656−1659.
(44) Blackburn, J. L.; McDonald, T. J.; Metzger, W. K.; Engtrakul, C.; Rumbles, G.; Heben, M. J. *Nano Lett.* **2008**, *8*, 1047.
(45) Zhou, W.; Vavro, J.; Nemes, N. M.; Fischer, J. E.; Borondics, F.; Kamarás, K.; Tanner, D. B. *Phys. Rev. B* **2005**, *71*, 205423.
(46) Strano, M. S.; Huffman, C. B.; Moore, V. C.; O'Connell, M. J.; Haroz, E. H.; Hubbard, J.; Miller, M.; Rialon, K.; Kittrell, C.; Ramesh, S.; Hauge, R. H.; Smalley, R. E. *J. Phys. Chem. B* **2003**, *107*, 6979.
(47) Kilina, S.; Tretiak, S. *Adv. Funct. Mater.* **2007**, *17*, 3405−3420.
(48) Tretiak, S.; Kilina, S.; Piryatinski, A.; Saxena, A.; Martin, R. L.; Bishop, A. R. *Nano Lett.* **2007**, *7*, 86−92.
(49) Niyogi, S.; Hamon, M. A.; Hu, H.; Zhao, B.; Bhowmik, P.; Sen, R.; Itkis, M. E.; Haddon, R. C. *Acc. Chem. Res.* **2002**, *35* (12), 1105−1113.
(50) Dewar, M. J. S.; Zoebisch, E. G.; Healy, E. F. *J. Am. Chem. Soc.* **1985**, *107*, 3902.
(51) Frisch, M. J.; Trucks, G. W.; Schlegel, H. B.; Scuseria, G. E.; Robb, M. A.; Cheeseman, J. R.; Scalmani, G.; Barone, V.; Mennucci, B.; Petersson, G. A.; Nakatsuji, H.; Caricato, M.; Li, X.; Hratchian, H. P.; Izmaylov, A. F.; Bloino, J.; Zheng, G.; Sonnenberg, J. L.; Hada, M.; Ehara, M.; Toyota, K.; Fukuda, R.; Hasegawa, J.; Ishida, M.; Nakajima, T.; Honda, Y.; Kitao, O.; Nakai, H.; Vreven, T.; Montgomery, J. A.; Peralta, J. E.; Ogliaro, F.; Bearpark, M.; Heyd, J.; Brothers, E.; Kudin, K. N.; Staroverov, N.; Kobayashi, R.; Normand, J.; Raghavachari, K.; Rendall, A.; Burant, J. C.; Iyengar, S. S.; Tomasi, J.; Cossi, M.; Rega, N.; Millam, J. M.; Klene, M.; Knox, J. E.; Cross, J. B.; Bakken, V.; Adamo, C.; Jaramillo, J.; Gomperts, R.; Stratmann, R. E.; Yazyev, O.; Austin, A. J.; Cammi, R.; Pomelli, C.; Ochterski, J. W.; Martin, R. L.; Morokuma, K.; Zakrzewski, V. G.; Voth, G. A.; Salvador, P.; Dannenberg, J. J.; .; Dapprich, S.; Daniels, A. D.; Farkas, O.; Foresman, J. B.; Ortiz, J. V.; Cioslowski, J.; Fox, D. J. *Gaussian 09*, revision A.01; Gaussian, Inc.: Wallingford, CT, 2009.
(52) Stewart, J. J. P. *J. Mol. Model.* **2007**, *13*, 1173.
(53) Tretiak, S.; Igumenshchev, K.; Chernyak, V. *Phys. Rev. B* **2005**, *71*, 33201.
(54) Becke, A. D. *J. Chem. Phys.* **1993**, *98*, 5648.
(55) Yanai, T.; Tew, D. P.; Handy, N. C. *J. Chem. Phys.* **2004**, *393*, 51.
(56) Martin, R. L. *J. Chem. Phys.* **2003**, *118*, 4775.
(57) Wu, C.; Malinin, S. V.; Tretiak, S.; Chernyak, V. Y. *Nat. Phys.* **2006**, *2* (9), 631−635.
(58) Tretiak, S.; Zhang, W. M.; Chernyak, V.; Mukamel, S. *Proc. Natl. Acad. Sci. U.S.A.* **1999**, *96*, 13003−13008.
(59) Pope, M.; Swenberg, C. E. *Electronic Processes in Organic Crystals*; Clarendon Press/Oxford University Press: Oxford/New York, 1982.
(60) Santos, S. M.; Yuma, B.; Berciaud, S.; Shaver, J.; Gallart, M.; Gilliot, P.; Cognet, L.; Lounis, B. *Phys. Rev. Lett.* **2011**, *107*, 187401.